



## RESEARCH ARTICLE OPEN ACCESS

# Mercury Detection in Novel Foods by a Smart Pocket Sensor

Iliaria Antonia Vitale<sup>+1</sup> | Giulia Selvolini<sup>+1</sup>  | Sara Failli<sup>1</sup> | Cristina Truzzi<sup>2</sup> | Giovanna Marrazza<sup>1</sup> <sup>1</sup>Department of Chemistry "Ugo Schiff" (DICUS), University of Florence, Sesto Fiorentino (FI), Italy | <sup>2</sup>Department of Life and Environmental Sciences (DISVA), Polytechnic University of Marche, Ancona, Italy**Correspondence:** Giovanna Marrazza ([giovanna.marrazza@unifi.it](mailto:giovanna.marrazza@unifi.it))**Received:** 16 May 2024 | **Revised:** 2 September 2024 | **Accepted:** 3 September 2024**Keywords:** mercury | nanocomposite | novel foods | smart sensor

## ABSTRACT

Mercury is one of the most well-known toxic contaminants of natural and anthropogenic origin in aquatic ecosystems that can bioaccumulate in vegetal and animal organisms. In this work, we propose a smart detection system for Hg(II) ions by square wave anodic stripping voltammetry at nanocomposite graphite screen-printed electrodes, as an analytical tool to be applied in food quality control. The nanocomposite surfaces were obtained by the modification of screen-printed graphite electrodes with poly(L-aspartic acid) and gold nanoparticles and were characterized by means of electrochemical techniques. An exhaustive study of the experimental conditions involved both in the electropolymerization and in the voltammetric stripping measurements was addressed to develop a reliable method capable of measuring Hg(II) concentration in the low  $\mu\text{g/L}$  range, both in conventional and drop configurations. The sensor was integrated in a smart setup, comprising a Sensit Smart pocket instrument connected to a smartphone, thus proving its applicability for *in situ* analysis due to its cost-effectiveness. The analytical significance of the developed sensor was assessed by detecting Hg(II) in novel food samples.

## 1 | Introduction

According to the Food and Agriculture Organization (FAO), the current food production will have to increase by at least the 60% by 2050 to meet the demands of the growing world population [1]: this necessity is one of the key drivers leading to the introduction of alternative foods in daily diet, together with increasing globalization, ethnic diversity and the search for new sources of nutrients [2]. Novel foods have been defined by the European Commission as "food that had not been consumed to a significant degree by humans in the EU before 15 May 1997", when the first novel food regulation came into force [3], and comprise foods with a new or intentionally modified primary molecular structure, foods isolated from microorganisms, fungi or algae, food isolated from plants or animals, and others [4]. Among these, algae and insects are

increasingly being introduced in Western societies as viable alternatives to animal proteins sources thanks to their rich nutritional content (proteins, fats, minerals, vitamins), lower request of land and water, and ability to grow on minimal nutrients [5].

However, since novel foods do not have a history of extensive consumption in Western industrialized countries, there is still a climate of insecurity about the related food safety because of the possible retention of contaminants [6]. For instance, food and feed consumption are one of the main pathways of exposure to heavy metals, which cause intoxication leading to diseases such as itai-itai (cadmium), saturnism (lead) and mercury poisoning. Contamination by mercury and its organic forms is one of the most critical issues due to the toxicity, persistence, and biological accumulation; environmental stud-

Authors with equal contribution

This is an open access article under the terms of the [Creative Commons Attribution](https://creativecommons.org/licenses/by/4.0/) License, which permits use, distribution and reproduction in any medium, provided the original work is properly cited.

© 2024 The Author(s). *Electroanalysis* published by Wiley-VCH GmbH.

ies assessing mercury bioaccumulation in insects can also provide interesting data [7–10]. In order to ensure the safe intake of novel foods and food in general, heavy metals and, specifically, mercury detection at trace levels results to be of utter importance. To reach this goal, electrochemical techniques show themselves to be promising for *in situ* analysis, because electrodes can be immersed into samples of interest with minimal perturbation [11], and to fulfil the 4S's criteria identified for a sensing probe to conform itself to: sensitivity, selectivity, size and speed [12]. Furthermore, screen-printed electrodes (SPEs) are in fact particularly suitable for *in situ* analysis due to both their small size and their cost effectiveness. Bare or modified screen-printed gold electrodes own a high affinity for Hg(II) and are usually chosen for inorganic mercury detection because the enhancement they provide in its preconcentration; moreover, the drawbacks caused by amalgam formation between gold and mercury are overcome, as SPEs do not require time-consuming cleaning treatments [13–16].

Gold-based nanomaterials have been also used as surface modifiers for carbon or graphite SPEs [17], allowing in some cases a further modification by immobilizing DNA strands for mercury recognition [18]. Kauffman's research group modified a screen-printed carbon electrode with gold nanoparticles by amperometry, detecting mercury up to 100 µg/L with a detection limit of 1.02 µg/L even in underground water [19]. In the study by Karapa *et al.* a plastic electrochemical sensor fabricated by injection molding was developed, and Au(III) was spiked into the samples and co-deposits with Hg(II) during the analysis to form an Au(Hg) amalgam *in situ*: mercury ions were also determined in complex matrices as honey, mussels tissue and fish oil with a detection limit of 0.4 µg/L [20]. Chen and collaborators have recently proposed an electrochemical sensor for mercury detection where gold nanoparticles and Hg were co-deposited on the electrode during the enrichment process, retrieving a limit of detection of 0.33 µg/L and applying the sensor in the analysis of drinking water samples [21].

In order to facilitate charge transfer between the electrode and the redox species, the modification of the electrodic surface with nanocomposite materials containing different types of organic or inorganic compounds has been extensively performed [22]; in particular, conductive polymers, as polyaniline

and its derivatives [23–25], alone or in combination with metal oxide nanoparticles [26], have shown good electrical conductivity, adhesion and adsorption ability towards Hg(II) [27, 28]. However, one critical point when dealing with this kind of polymers is about the carcinogenicity related to their monomers; therefore, nontoxic, biocompatible and biodegradable alternatives such amino acids have drawn a lot of attention in the last few years due to their advantages, including electrochemical stability and a wide number of side functional groups [29]. Moreover, recognition layers formed by amino acids grafted onto the working electrodes were also developed for metal ions detection, for the strong interaction established between the modified surface and the analytes, thus enhancing the performance of the electrochemical platform [30].

Taking into account all the aforementioned considerations, this work aims to present a nanocomposite electrochemical platform for the determination of Hg(II) in novel foods samples, such as algae and house cricket flour (*Acheta domesticus*, recently authorized by the EU as *novel food* [31]). In particular, poly(L-aspartic acid) (p(L-Asp)) was combined with gold nanoparticles (AuNPs) to form a sensing layer onto graphite screen-printed electrodes (GSPEs), increasing their electroactive surface area and enhancing their sensitivity for mercury detection by means of square wave anodic stripping voltammetry (SWASV).

As far as we know, none of the previously cited studies made use of GSPEs modified with a polyaminoacid and noble metal nanoparticles for mercury detection. In this regard, even if the use of conducting polymers and gold nanoparticles, although employed separately as working electrode modifiers, is not new in detecting mercury, the main novelty of this work relies in the application of the developed platform in the analysis of real samples deriving from seaweeds and insects.

Testing these complex matrices is a crucial point in determining the applicability of the sensor for food quality control purposes, also considering the increasingly spreading of novel foods in the worldwide diet. Keeping this aim in mind, both the modification and detection steps were accurately studied to retrieve the optimal detection conditions for mercury in the aforementioned samples. Moreover, the present study shows lower detection limit and analysis time if compared to the reported bibliographic findings (Table 1).

**TABLE 1** | Analytical details of the reported studies on mercury determination with gold nanomaterials-modified carbon screen-printed electrodes.

Working electrode	Modification	LOD (µg/L)	Linear range (µg/L)	Analysis time (min)	Real samples	Ref.
Carbon SPE	AuNPs	1.02	1–100	≈ 6	Underground water	[19]
Carbon SPE	Au(Hg) amalgam	0.4	1.2–80	≈ 8	Honey, mussels tissue and fish oil	[20]
Carbon SPE	Au(Hg) amalgam	0.33	0.5–80	≈ 5	Drinking water	[21]
GSPE	AuNPs/p(L-Asp)	0.24	5–25	≈ 1	Seaweeds and house cricket flour	This work

## 2 | Materials and Methods

### 2.1 | Chemicals

Hg(II) atomic absorption standard – 1000 mg/L in nitric acid (HNO<sub>3</sub>), diluted as required in 0.5 M HNO<sub>3</sub>; l-aspartic acid (l-Asp); tetrachloroauric acid (HAuCl<sub>4</sub>); sulfuric acid (H<sub>2</sub>SO<sub>4</sub>); sodium chloride (NaCl); potassium chloride (KCl); potassium ferrocyanide (K<sub>4</sub>[Fe(CN)<sub>6</sub>]); potassium ferricyanide (K<sub>3</sub>[Fe(CN)<sub>6</sub>]); hexaammineruthenium(II) chloride ([Ru(NH<sub>3</sub>)<sub>6</sub>]Cl<sub>2</sub>), hexaammineruthenium(III) chloride ([Ru(NH<sub>3</sub>)<sub>6</sub>]Cl<sub>3</sub>), di-sodium hydrogen phosphate (Na<sub>2</sub>HPO<sub>4</sub>); sodium di-hydrogen phosphate (NaH<sub>2</sub>PO<sub>4</sub>). All reagents were purchased from Merck (Darmstadt, Germany). All solutions were prepared with Milli-Q water (resistivity: 18 MΩ).

### 2.2 | Apparatus

A PalmSens portable potentiostat/galvanostat and a Sensit Smart pocket potentiostats/galvanostat (PalmSens BV, Houten, The Netherlands), controlled by PSTrace 5.9 software or PSTouch application, respectively, for data acquisition and elaboration, were used for performing the electrochemical measurements, which were conducted at room temperature. Specifically, the modification and characterization steps were performed with PalmSens, while the detection step was performed by using Sensit Smart. The experiments were carried out on screen-printed electrochemical cells (EcoBioServices srl, Sesto Fiorentino (FI), Italy) based on a graphite working electrode, a graphite counter electrode, and a silver pseudo-reference electrode, to which all the reported potentials refer. Scanning electron microscopy (SEM) analysis was performed with a Gaia 3 microscope (Tescan a.s., Brno, Czech Republic). SEM morphologies were acquired using an acceleration voltage of 20 kV. Energy dispersive X-ray analysis (EDX) was performed to assess the elemental composition of the modified electrode surface.

### 2.3 | Electrodes Modification

Graphite screen-printed electrodes (GSPEs) were modified by electrodeposition of a film of poly(l-aspartic acid) (p(l-Asp)) by cyclic voltammetry (CV) and gold nanoparticles (AuNPs) by amperometry; the nanocomposite-modified electrodes were addressed as AuNPs/p(l-Asp)/GSPE.

Briefly, the electropolymerization was conducted by dropping 50 μL of a 2 mM l-Asp solution in 0.05 M phosphate buffer solution (PBS) pH 7.4, containing 0.1 M NaCl, and by scanning the potential from +1.0 V to +1.7 V for 20 cycles at 100 mV/s. Electrodeposition of AuNPs was then performed onto the polymer-modified surfaces (p(l-Asp)/GSPE) by dropping 50 μL of a 0.5 mM HAuCl<sub>4</sub> solution in 0.5 M H<sub>2</sub>SO<sub>4</sub> and by applying a potential of –0.2 V for 130 s.

Finally, the nanocomposite-modified platforms were rinsed with Milli-Q water and let dry at room temperature before use.

### 2.4 | Study of the Electrochemical Performance of AuNPs/p(l-Asp)/GSPE

To gain insights into the nanostructuring of the electrode surface, and especially into its influence on the electrochemical performance of the screen-printed cells, CV measurements were performed on the modified GSPEs at different scan rates (25, 50, 75, 100, 125, 150, 175 mV/s) after each step of modification by dropping 50 μL of 5 mM [Fe(CN)<sub>6</sub>]<sup>4/–3</sup> redox probe (equimolar solution prepared in 0.1 M KCl) and scanning the potential in a range comprised between –1.0 V and +1.0 V. The current peak height (*i<sub>p</sub>*) of both cathodic and anodic peaks was plotted against the square root of the scan rate (*v*<sup>1/2</sup>). The obtained curves were fitted with the Randles-Sevcik equation [32]:

$$i_p = (2.69 \times 10^5) n^{3/2} A c (D v)^{1/2} \quad (1)$$

where *n* is the number of electrons transferred in the redox event, *A* (cm<sup>2</sup>) is the electroactive surface area, *c* (mol/cm<sup>3</sup>) is the probe bulk concentration and *D* (cm<sup>2</sup>/s) is the diffusion coefficient for the oxidized analyte. A further voltammetric characterization was performed in presence of the positively-charged [Ru(NH<sub>3</sub>)<sub>6</sub>]<sup>+2/+3</sup> redox probe (1 mM equimolar solution prepared in 0.1 M KCl) in the same scan rate conditions and scanning the potential in a range comprised between –0.55 V and +0.05 V. Electrochemical impedance spectroscopy (EIS) measurements were also performed in presence of 5 mM [Fe(CN)<sub>6</sub>]<sup>4/–3</sup> redox probe (equimolar solution prepared in 0.1 M KCl) by scanning the frequency in the range 100 kHz–10 mHz with an amplitude of 10 mV at a fixed DC potential of +0.13 V. EIS spectra, presented in the form of complex plane diagrams (*i.e.*, Nyquist plots), were fitted with the proper equivalent circuit (Figure 1), while charge transfer resistance (*R<sub>ct</sub>*) values were taken as analytical signals.

EIS measurements were also performed for each modification step at different concentrations (0.1, 0.2, 0.5, 1, 2, 5 mM) of [Fe(CN)<sub>6</sub>]<sup>4/–3</sup> redox probe (equimolar solution prepared in 0.1 M KCl). The obtained *R<sub>ct</sub>* values were plotted against the inverse of the concentration (1/*C*) and the resulting curves were fitted with the following equation [33]:

$$R_{ct} = \frac{RT}{n^2 F^2 A k^0} \cdot 1/C \quad (2)$$

where *R* (8.3145 J/(mol·K)) is the gas constant, *T* (K) is the temperature, *n* is the number of electrons transferred in the

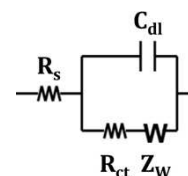


**FIGURE 1** | Randles equivalent circuit used to fit EIS measurements (*R<sub>s</sub>*: electrolyte resistance, *C<sub>dl</sub>*: double layer capacitance, *R<sub>ct</sub>*: charge transfer resistance, *Z<sub>w</sub>*: Warburg impedance).

redox event,  $F$  (96500 C/mol) is the Faraday constant,  $A$  ( $m^2$ ) is the electroactive surface area and  $k^0$  (cm/s) is the electron transfer rate constant.

The thus tested SPEs were discarded after each CV or EIS measurement.

## 2.5 | Voltammetric Stripping Determination of Hg(II) at Nanocomposite-Modified Electrodes

Hg(II) calibration curve at the nanocomposite AuNPs/p(l-Asp)/GSPEs platforms was performed by means of square wave anodic stripping voltammetry (SWASV) in a mixture of 10 mM  $HNO_3$  and 10 mM NaCl as the supporting electrolyte solution. SWASV measurements were carried out by applying a deposition potential ( $E_{dep}$ ) of  $-0.4$  V for a deposition time ( $t_{dep}$ ) of 30 s in order to promote the accumulation of the mercury on the nanocomposite platform surface under stirring conditions; the  $t_{dep}$  was increased up to 180 s under drop conditions. After an equilibration time of 10 s, SWASV curves were recorded between  $+0.2$  V and  $+0.8$  V with a frequency of 25 Hz, a potential step of 2.5 mV and an amplitude of 10 mV.

Concerning the conventional configuration, stripping measurements were performed by immersing the screen-printed cells in 5 mL of the supporting electrolyte, where mercury concentration was increased by consecutive additions of a 5 mg/L standard solution. Concerning the drop configuration, stripping measurements were performed by consecutively dropping 50  $\mu$ L of different solutions at increasing concentration of Hg(II) onto the screen-printed cells; after each stripping scan, the dropped solution was discarded. Each mercury determination is reported as the average of at least three different measurements. The sensitivity of the method was determined from the slope of the calibration curve and the limit of detection (LOD) was computed as three times the standard deviation of the blank divided by the slope of the calibration curve. The inter-assay reproducibility was evaluated by calculating the percentage relative standard deviation (%RSD) from at least ten independent measurements on different screen-printed cells.

## 2.6 | Analysis of Novel Food Samples

Different types of red (*Porphyra dioica*, *P. yezoensis* – also known as *nori* – and *Palmaria palmata*) and brown algae (*Undaria pinnatifida* – also known as *wakame* – and *Ascophyllum nodosum*), used both for human consumption and animal feeding (e.g., *Acheta domesticus* [34]) and *Acheta domesticus* flour were chosen as increasingly-used examples of novel foods.

A portion of each food powder was mixed with a solution of  $HNO_3/H_2O_2$  1:1 and a mineralization was performed in a microwave oven. The samples were initially irradiated for 20 min, to raise their temperature from  $20^\circ C$  to  $200^\circ C$ ; then, a maximum power of 1600 W maintained the temperature constant at  $200^\circ C$  for at least 3 h. The resulting suspensions were filtered and diluted at a proper ratio in the supporting

electrolyte. Mercury determination was performed by spiking the obtained extracts with Hg(II) standard solutions and by performing stripping analysis under the same experimental conditions as previously reported.

## 3 | Results and Discussion

### 3.1 | Optimization of p(l-Asp) and AuNPs Electrodeposition

Poly(l-aspartic acid) can be easily deposited by means of CV onto carbon-based electrodes by electrooxidation of its monomer, where the resulting radical could link to the electrode surface and then form a polymeric layer rich in negatively charged groups [35], which could also be exploited for the immobilization of several bioreceptors.

The properties of the electrodeposited film can be easily tuned by varying its thickness, which can be realized by controlling the amount of charge passing during the polymerization event; therefore, the optimization of the voltammetric parameters results to be of outstanding importance.

For this purpose, l-Asp was polymerized onto GSPEs at different concentrations of l-Asp precursor (0.5, 1, 2 and 5 mM) and using a different number of cycles (10, 15, 20, 25, 30) and the modified electrodes were characterized by means of CV and EIS (Figure 2 and Figure 3).

The obtained current peak heights and charge transfer resistance values follow two opposite and complementary behavior, as the first has a maximum when [l-Asp] is equal to 2 mM, that is the value where the second shows a minimum. Therefore, this concentration was used for l-Asp polymerization in all the subsequent experiments.

From the reported voltammograms, it can be observed that the current peak height increased with increasing the number of cycles for the polymerization, while Nyquist plots show that

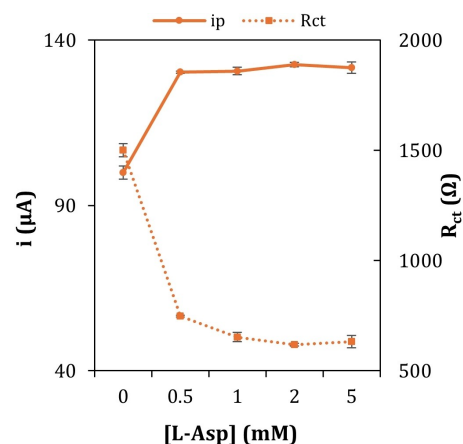


**FIGURE 2** | Peak current and  $R_{ct}$  values of poly(l-aspartic acid)-modified GSPEs in 5 mM  $[Fe(CN)_6]^{4-/3-}$  (equimolar solution prepared in 0.1 M KCl) at different l-Asp concentrations (polymerization cycles: 20).

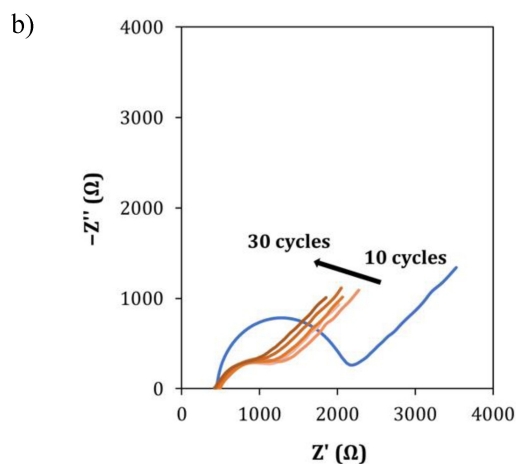
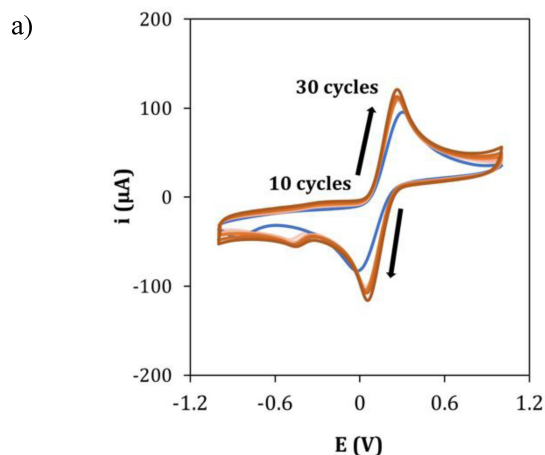


**FIGURE 3** | a) CV and b) EIS characterization of • bare and • poly(l-aspartic acid)-modified GSPEs in 5 mM  $[\text{Fe}(\text{CN})_6]^{4-/3-}$  (equimolar solution prepared in 0.1 M KCl) at different polymerization cycles ( $[\text{l-Asp}] = 2 \text{ mM}$ ).

the diameter of the circular portion of the curve (related to the charge transfer resistance,  $R_{ct}$ ) exhibits an opposite behavior, as it decreased with increasing the number of cycles. A further CV and EIS comparison was also performed between polymer-modified GSPEs, with 20 and 30 cycles of polymerization, after the electrodeposition of gold nanoparticles for 130 s (Figure S1).

As it is clear from both graphs, no difference can be appreciated between the platforms built with l-Asp polymerized for 20 or 30 cycles; therefore, for the sake of quickness, 20 cycles were used for the electropolymerization in all the subsequent experiments.

To complete the optimization process of the nanostructured platform, different concentrations of  $\text{HAuCl}_4$  precursor (0.05, 0.1, 0.2 and 0.5 mM) and amperometry times (70, 100, 130, 160, 190 s) for the deposition of gold nanoparticles were also used and the resulting platforms were characterized with CV and EIS as shown until now (Figure 4 and Figure 5).

The current peak heights increase with increasing concentrations of the precursor, while the charge transfer resistance

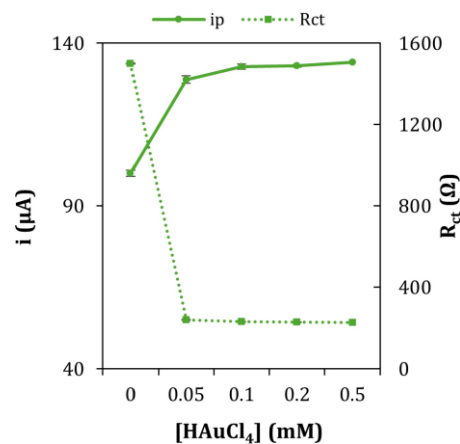


**FIGURE 4** | Peak current and  $R_{ct}$  values of AuNPs/p(l-Asp)/GSPEs in 5 mM  $[\text{Fe}(\text{CN})_6]^{4-/3-}$  (equimolar solution prepared in 0.1 M KCl) at different  $\text{HAuCl}_4$  concentrations (amperometry time: 130 s).

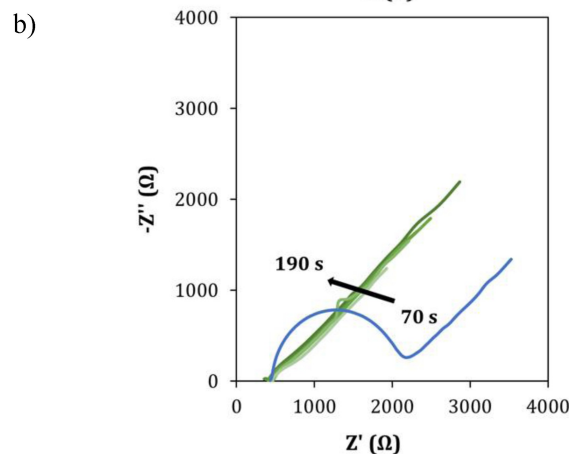
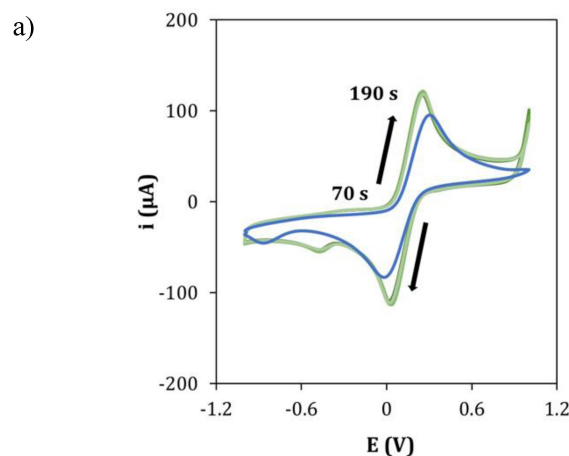


**FIGURE 5** | a) CV and b) EIS characterization of • bare and • AuNPs/p(l-Asp)/GSPEs in 5 mM  $[\text{Fe}(\text{CN})_6]^{4-/3-}$  (equimolar solution prepared in 0.1 M KCl) at different gold deposition times ( $[\text{HAuCl}_4] = 0.5 \text{ mM}$ ).

follows again an opposite behavior: therefore, 0.5 mM was used to electrodeposit gold nanoparticles in all the subsequent experiments.



As already happened previously (Figure S1), no appreciable difference can be observed between the nanocomposite platforms where gold was electrodeposited for different times; therefore, to find a compromise between retrieving a good conductivity and avoiding exceeding in the amount of the metal, 130 s was chosen as the electrodeposition time for gold nanoparticles and was used for all the subsequent experiments.

The nanostructured platform obtained under the optimized conditions was characterized by CV in 0.1 M KCl solution (Figure S2).

The obtained voltammetric scans clearly show the presence of redox peaks when gold is electrodeposited either on bare graphite or polymer-modified GSPEs, thus confirming the presence of AuNPs on the electrodic surface. A further characterization was also performed by means of SEM and EDX to assess for the morphology and the composition of the surface (Figure 6).

SEM morphology confirms the presence of AuNPs, which are randomly distributed on the surface of the working electrode; moreover, EDX analysis was carried out to assess the effective

modification of the electrodes, which was confirmed by the presence of a characteristic gold band around 2.2 keV.

### 3.2 | Electrochemical Performance of the Nanocomposite Platform

The optimized nanocomposite platform comprising poly(l-aspartic acid) and gold nanoparticles was electrochemically characterized in all its assembly steps by performing cyclic voltammograms at different scan rates in presence of the reversible redox couple  $[\text{Fe}(\text{CN})_6]^{4-/3-}$  to assess for an enhancement of the electrochemical performance of the graphite working electrode after the modification procedure.

The cyclic voltammograms obtained for bare and modified GSPEs are shown in Figure 7.

As it can be observed, an increase in the current peak height, both in oxidation and in reduction, is retrieved by comparing the nanocomposite-modified electrochemical platform with the bare graphite working electrode, as poly(l-aspartic acid) and gold nanoparticles fostered the electron transfer between the redox probe and the electrode surface.

Moreover, the scan rate study shows that both the anodic ( $i_{pa}$ ) and the cathodic ( $i_{pc}$ ) peak current increased with increasing the scan rate from 25 mV/s to 175 mV/s (Figure S3).

A good linearity was obtained between the  $i_p$  values and the square root of the scan rate, suggesting that the electron transfer process was controlled by diffusion. These linear relationships also confirmed that the electrochemical processes occurring at the electrode surface are kept efficient and confined to the surface after the modification with the nanocomposite film, which does not hinder the electron transfer but, instead, favors it.

The electroactive surface area could be then calculated for each assembly step by applying the Randles-Sevcik equation to the angular coefficient of the linear regressions previously retrieved after plotting the current peak height vs. the square root of the scan rate. The obtained values are reported in Table 2.

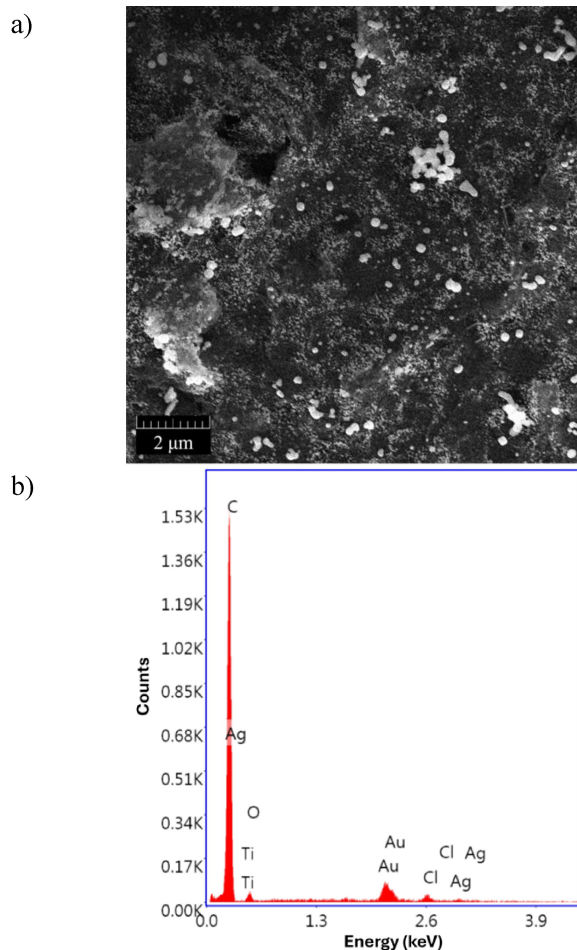


**FIGURE 6** | Microscopic characterization of the nanostructured platform. (a) SEM morphology of AuNPs/p(l-Asp)/GSPEs and (b) EDX spectrum of AuNPs/p(l-Asp)/GSPEs.

**TABLE 2** | Electroactive area values calculated with the Randles-Sevcik equation for all the building steps of the nanocomposite platform.

	GSPE	p(l-Asp)/GSPE	AuNPs/p(l-Asp)/GSPE
Anodic area (mm <sup>2</sup> )	4.8	2.9	6.2
Cathodic area (mm <sup>2</sup> )	4.1	3.3	5.9
Average area (mm <sup>2</sup> )	4.5	3.1	6.1
Standard deviation (mm <sup>2</sup> )	0.5	0.3	0.2

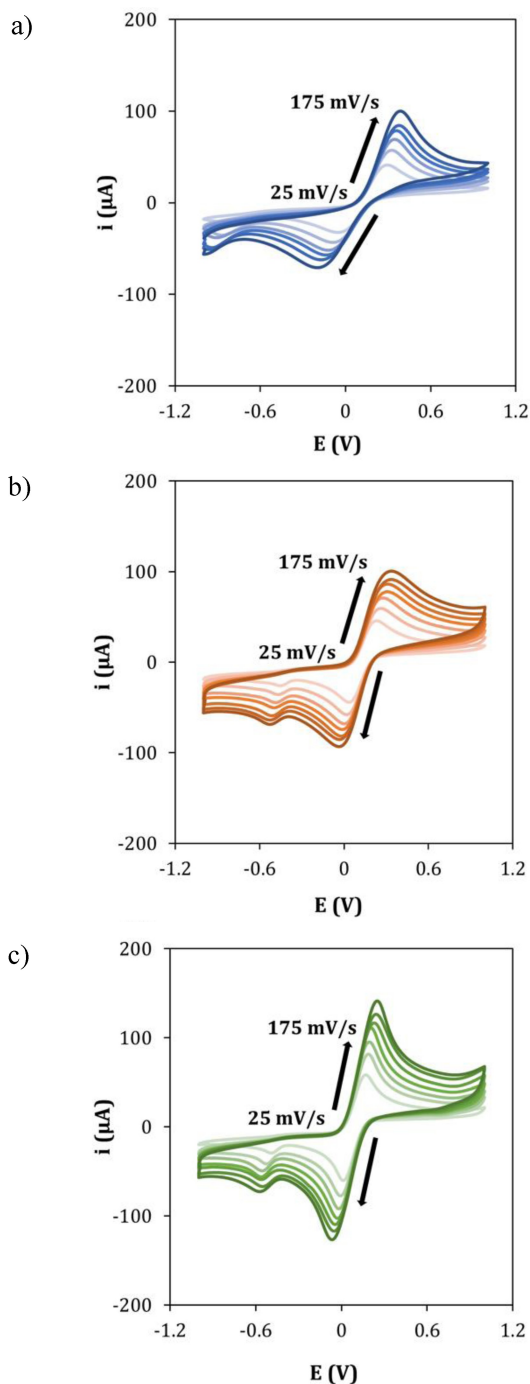


**FIGURE 7** | CV characterization of unmodified GSPEs and nanocomposite-modified GSPEs in 5 mM  $[\text{Fe}(\text{CN})_6]^{-4/-3}$  (equimolar solution prepared in 0.1 M KCl) at different scan rates. a) GSPEs; b) p(l-Asp)/GSPEs; c) AuNPs/p(l-Asp)/GSPEs.

The calculated electroactive area values confirmed that the nanocomposite-modified electrodes showed the faster charge transfer behavior previously demonstrated by the cyclic voltammograms reported in Figure 7. Regarding the modification of GSPEs with the sole poly(l-aspartic acid), the electroactive area resulted to be smaller than that related to the bare electrodes; even if the use of the polymer gave reproducibility and reversibility to the surface (as it can also be observed from

the reduction in the potential peak separation when passing from GSPEs to p(l-Asp)/GSPEs), its presence may have established an electrostatic repulsion between the carboxylic groups of the polymer and the negatively charged redox probe, which led to a decrease in the area with respect to the unmodified GSPEs. Even if these findings seem to be somehow in contrast between each other, it may be possible that the similarities between the CV peaks before and after the electro-polymerization are due to a counterbalance between two effects: the increase of the current brought by the increase of the nanostructuring after the polymer formation, and the decrease of the current brought by the aforementioned electrostatic repulsion. A further confirmation was retrieved when repeating the scan rate study in presence of the positively-charged redox probe  $[\text{Ru}(\text{NH}_3)_6]^{+2/+3}$  for all the assembly steps of the nanostructured platform (Figure 8).

As it can be seen from the reported voltammograms, the increase in both anodic and, especially, cathodic current peak heights retrieved when comparing the polymer-modified surface with the bare graphite working electrode is more pronounced than that obtained in the study performed with  $[\text{Fe}(\text{CN})_6]^{-4/-3}$ . This could be explained this time with the establishment of an electrostatic attraction between the carboxylic groups of the polymer and the positively charged redox probe. The aforementioned findings were also confirmed by the results of EIS measurements, as they are complementary to those given by CV: in fact, the  $R_{ct}$  values of the electrode modified with both the nanostructured materials (0.2 k $\Omega$ ) decreased significantly with respect both to the polymer-modified GSPE (0.7 k $\Omega$ ) and to the unmodified GSPE (1.8 k $\Omega$ ), as shown in Figure 9.

As a further confirmation of the above-mentioned results, EIS measurements were also performed at different concentrations of  $[\text{Fe}(\text{CN})_6]^{-4/-3}$  redox probe to calculate the electron transfer rate constant. The Nyquist plots obtained for bare and modified GSPEs are shown in Figure S4.  $k^0$  could be then calculated for each assembly step by applying the Equation (2) to the angular coefficient of the linear regressions previously retrieved after plotting the  $R_{ct}$  values vs. the inverse of the concentration of the redox probe. The calculated  $k^0$  values ( $6.72 \cdot 10^{-4}$  cm/s for GSPEs,  $2.44 \cdot 10^{-3}$  cm/s for p(l-Asp)/GSPEs and  $4.13 \cdot 10^{-3}$  cm/s for AuNPs/p(l-Asp)/GSPEs) confirmed once more the faster charge transfer behavior previously demonstrated for the nanocomposite-modified electrodes.

### 3.3 | Optimization of the Experimental Conditions for Stripping Analysis

Searching for a compromise between an improvement of the analytical response and a decrease of the analysis time, key experimental parameters, as the deposition time ( $t_{dep}$ ) and the deposition potential ( $E_{dep}$ ), were assessed upon the Hg(II) stripping signal. The optimization of  $t_{dep}$  was performed at an  $E_{dep}$  of  $-0.4$  V by varying Hg(II) concentration in the range 5–25  $\mu\text{g/L}$  and by depositing mercury ions for 15 s, 30 s or 45 s; Table 3 shows the analytical features of the calibration curves obtained for each one of the selected values.

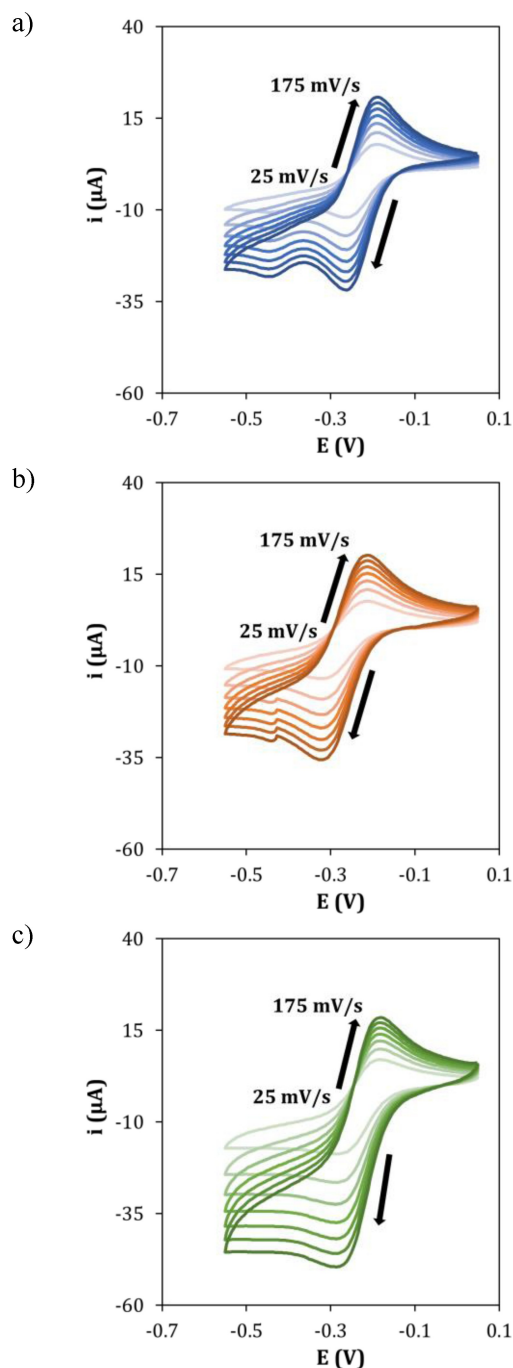


**FIGURE 8** | CV characterization of unmodified GSPEs and nano-composite-modified GSPEs in 1 mM  $[\text{Ru}(\text{NH}_3)_6]^{+2/+3}$  (equimolar solution prepared in 0.1 M KCl) at different scan rates. a) GSPEs; b) p(I-Asp)/GSPEs; c) AuNPs/p(I-Asp)/GSPEs.

From the reported results, it can be noted that – consistently with the principle of the technique – the sensitivity of the method increases with increasing the deposition time, together with the maximum value of the percentage relative standard deviation (%RSD) related to the datapoints of the linear regressions. The advantages brought by these two opposite trends meet together when using 30 s as  $t_{\text{dep}}$ , when the lowest LOD was also retrieved: therefore, this value for  $t_{\text{dep}}$  was used for all the subsequent experiments. In a similar manner, the optimization of  $E_{\text{dep}}$  was performed at a  $t_{\text{dep}}$  of 30 s by varying

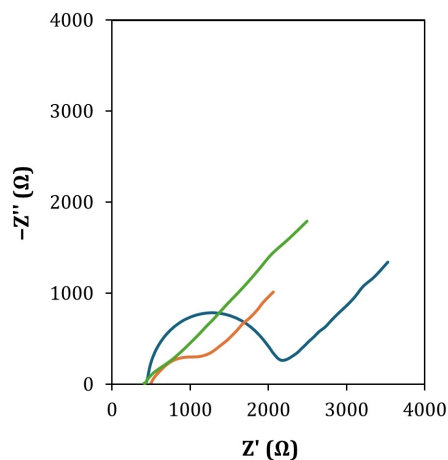


**FIGURE 9** | EIS characterization of unmodified GSPEs and nano-composite-modified GSPEs in 5 mM  $[\text{Fe}(\text{CN})_6]^{-4/-3}$  (equimolar solution prepared in 0.1 M KCl): • GSPEs; • p(I-Asp)/GSPEs; • AuNPs/p(I-Asp)/GSPEs.

**TABLE 3** | Analytical parameters of mercury calibration curves obtained at deposition potential of  $-0.4$  V and deposition times of 15 s, 30 s and 45 s ( $n = 3$ ).

	$t_{\text{dep}} =$ 15 s	$t_{\text{dep}} =$ 30 s	$t_{\text{dep}} =$ 45 s
Sensitivity (mA·L/g)	15.3	20.8	32.8
$R^2$	0.9985	0.9982	0.9969
LOD ( $\mu\text{g/L}$ )	0.34	0.24	0.60
%RSD <sub>max</sub>	8.5	14.3	23.4

**TABLE 4** | Analytical parameters of mercury calibration curves obtained at deposition time of 30 s and deposition potentials of  $-0.3$  V,  $-0.4$  V and  $-0.5$  V ( $n = 3$ ).

	$E_{\text{dep}} =$ $-0.3$ V	$E_{\text{dep}} =$ $-0.4$ V	$E_{\text{dep}} =$ $-0.5$ V
Sensitivity (mA·L/g)	13.2	20.8	29.4
$R^2$	0.9946	0.9982	0.9384
LOD ( $\mu\text{g/L}$ )	1.10	0.24	1.01
%RSD <sub>max</sub>	22.8	14.3	32.9

Hg(II) concentration in the range 5–25  $\mu\text{g/L}$  and by depositing mercury ions at  $-0.3$  V,  $-0.4$  V or  $-0.5$  V; Table 4 shows the analytical features of the calibration curves obtained for each one of the selected values.

The obtained results show that a higher sensitivity was retrieved when using a lower deposition potential: however, the %RSD values, together with the LOD values, are higher if using an  $E_{\text{dep}}$  different from  $-0.4$  V. Therefore, an  $E_{\text{dep}}$  of  $-0.4$  V was used in all the following experiments.



### 3.4 | Mercury Detection by SWASV

The evaluation of the analytical performance was conducted by means of SWASV calibration of mercury performed in triplicate by using a new nanostructured GSPE in each replicate. Calibration curves were obtained by measurements carried out under the optimized conditions: the analyzed Hg(II) concentrations increased from 0  $\mu\text{g/L}$  to 50  $\mu\text{g/L}$ , while a linear response was retrieved in the range 0–25  $\mu\text{g/L}$ . The oxidation peak of mercury observed around +0.46 V increased linearly with the metal concentration. The obtained voltammograms, together with the resulting calibration curve are shown in Figure 10.

With the aim of highlighting the improvements of the nanostructured electrode for Hg(II) detection, the whole stripping procedure was repeated at bare and one component-modified graphite electrodes (that is, p(l-Asp)/GSPE and AuNPs/GSPE). While bare and polymer-modified electrodes were not able to properly detect mercury, a stripping peak could be observed when testing gold-modified GSPEs, due to the fact of an amalgam formation between the analyte and the noble metal, as previously mentioned in section 1.

The SWAS voltammograms obtained in these conditions are shown in Figure S5. A clear potential shift towards more

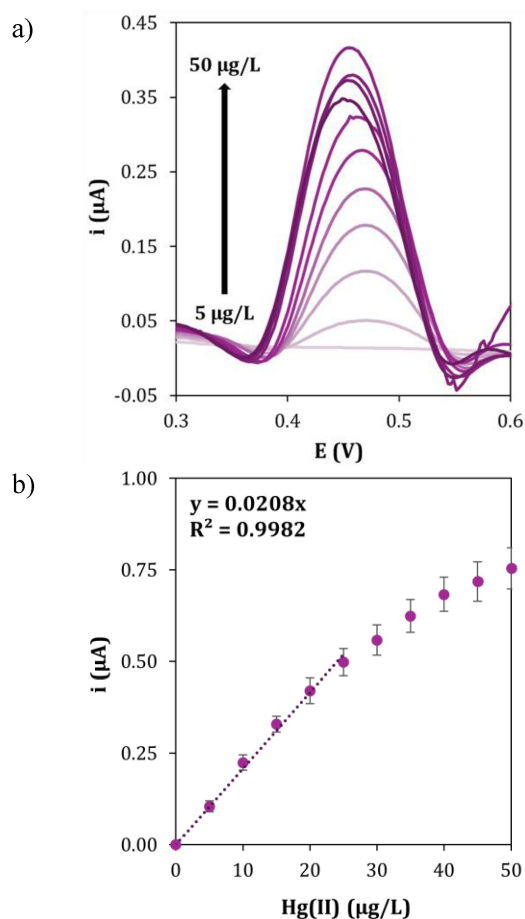


**FIGURE 10** | a) SWAS voltammograms at AuNPs/p(l-Asp)/GSPE for increasing concentration of mercury and b) corresponding calibration curve ( $n = 3$ ).

negative values can be observed when mercury concentration increases, together with a consistent variation of the baseline obtained when analyzing the blank solution; moreover, no definite mercury peak could be detected for concentrations lower than 5  $\mu\text{g/L}$ , and the saturation of the signal occurs at a lower mercury concentration (15  $\mu\text{g/L}$ ) with respect to that occurring with AuNPs/p(l-Asp)/GSPE platform (25  $\mu\text{g/L}$ ).

The detection limit of 0.24  $\mu\text{g/L}$  for mercury was calculated from the  $3 \cdot s_b/m$  criterion, where  $s_b$  is the blank standard deviation and  $m$  is the slope of the calibration plot. Under optimal conditions, the reproducibility of the AuNPs/p(l-Asp)/GSPEs platform was also studied by performing ten calibration curves for Hg(II) in the supporting electrolyte and evaluating the variation in the sensitivity (*i.e.*, the slope of the calibration curve). A highly stable response along ten consecutive measurements was obtained with a %RSD of 9%, thus proving that the nanocomposite-modified GSPEs own a high reproducibility.

#### 3.4.1 | Drop Analysis

The use of screen-printed cells has significantly increased in several fields as clinical, environmental and food control chemistry because of their low cost due to mass production and of the miniaturization allowed by their small dimensions; all these features make them particularly attractive for performing rapid and *in situ* analysis [36].

Therefore, in order to develop a portable device and to simplify the experimental setup, drop measurements were performed by dropping onto the nanocomposite-modified GSPEs solutions containing an increasing concentration of Hg(II) up to 50  $\mu\text{g/L}$ ; SWASV scans were then performed under the optimized experimental conditions. However, since the stirring conditions are usually present in stripping analysis to promote the accumulation of the metal onto the electrodic surface, a drop configuration could somehow hamper the diffusion processes occurring in solution. In fact, the deposition time of 30 s, which resulted to be the optimal parameter for Hg(II) analysis in the conventional configuration, was not sufficient in the case of drop measurements. Further tests were then performed by increasing the  $t_{dep}$  up to 180 s, which resulted to be the optimal one for this configuration, as the corresponding calibration curve owns the highest sensitivity and  $R^2$ , with low standard deviation values (data not shown).

The voltammograms obtained under these new conditions, together with the corresponding calibration curve, are shown in Figure 11.

From the obtained results, the sensitivity decreased down to almost the 16% of that obtained in the conventional configuration; moreover, the detection limit of 0.62  $\mu\text{g/L}$  is higher than that retrieved previously. On the other side, a linear correlation was retrieved between the current peak height and the concentration of mercury up to 50  $\mu\text{g/L}$  without any saturation of the electrode surface. These phenomena are also consistent with what was already observed for the stripping analysis of other metals [37].

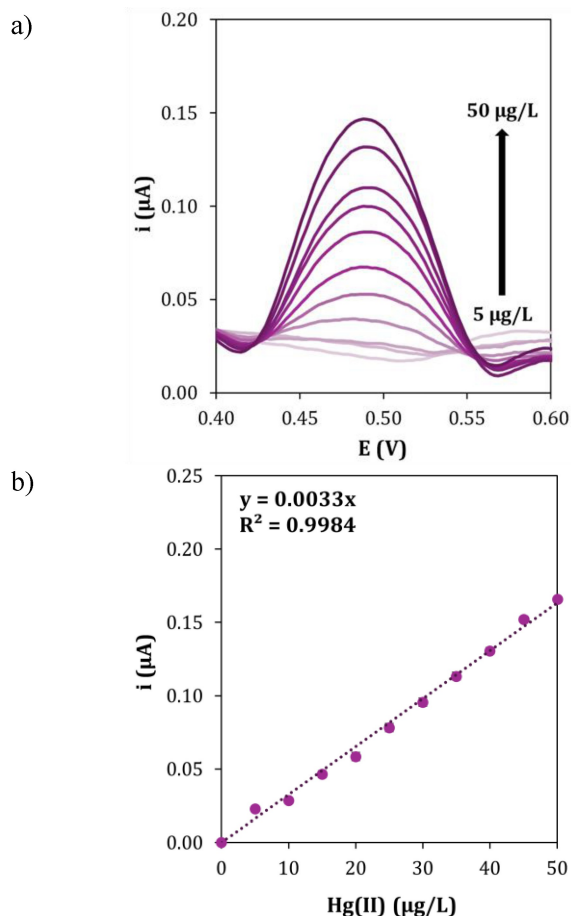


**FIGURE 11** | a) SWAS voltammograms at AuNPs/p(l-Asp)/GSPE for increasing concentration of mercury and b) corresponding calibration curve ( $n = 3$ ) in drop configuration.

### 3.5 | Selectivity

As some frequently occurring metal ions such as Cd(II), Cu(II), Pb(II) and Zn(II) could potentially interfere in the determination of Hg(II) by SWASV at AuNPs/p(l-Asp)/GSPEs. In fact, these metal ions could compete with mercury in the formation of an amalgam with gold nanoparticles or generate further reduction peaks that overlap with that of the analyte. Therefore, experiments were performed to assess the extent of this interference.

Mercury stripping analysis was performed in presence of 15 µg/L of Hg(II) and each one of the aforesaid metals at concentrations of 100-fold and 500-fold, both in conventional and drop configuration. The obtained stripping current values ( $i_{\text{Hg(II)}+M(\text{II})}$ ) were thus compared with those retrieved in absence of any interferent metal ( $i_{\text{Hg(II)}}$ ), as shown in Table 5.

As it can be observed from the reported values, the influence of the metals on Hg(II) signal is variable, even if no additional peaks could be detected in the obtained voltammograms along the potential range used for the stripping scan. Lead excesses had a strong influence on Hg(II) signal, causing an average 80% increase for the conventional stripping analysis, while an average 70% increase for drop analysis. Almost independently

from the configuration, cadmium caused an average 25% variation in the stripping current of mercury, while at higher concentrations this increase raised up to the 35%. Copper caused a substantial increase of Hg(II) stripping current in the conventional configuration both at 100- and 500-fold concentrations, while the situation is inverted in drop configuration, when no significant effect was observed. Lastly, zinc caused a negligible effect regardless its concentration, both in conventional and drop configuration.

### 3.6 | Real Samples Analysis

The applicability of the proposed method in the development of a smart setup for food quality control was evaluated by analyzing several complex matrices deriving from novel food samples, such as seaweeds and cricket flour. The samples were pretreated as reported in section 2.6; the determination of mercury was carried out after diluting the samples to a proper ratio, by spiking them with increasing concentrations of Hg(II) in the same range of the calibration curve in standard solutions and by performing SWASV measurements under the optimized conditions in drop configuration. The obtained results are shown in Table 6.

As it can be observed from the reported values, the sensitivity values for mercury determination in the selected matrices is comparable to those obtained from the calibration curve in standard solutions (section 3.4.1), both in red and brown algae, which could be a promising element for mercury detection in contaminated novel foods, the analysis of which could even strengthen the aforementioned results. However, a reduction in the sensitivity was retrieved in the case of mercury determination in cricket flour extract; this effect may be due to a higher complexity of the animal matrix compared to the vegetal ones that may exert a stronger influence on mercury detection.

## 4 | Conclusions

In this work, a nanocomposite made up by poly(l-aspartic acid) (p(l-Asp)) and gold nanoparticles (AuNPs) was directly electro-deposited onto the surface of commercial graphite screen-printed electrodes (GSPEs): the developed electrochemical platform was studied by CV and EIS techniques and then tested for the determination of Hg(II) by SWASV. An optimization step of the electrochemical parameters related both to the electropolymerization of the aminoacid and the preconcentration of mercury ions was performed; then, calibration curves were obtained under the application of a deposition potential of  $-0.4$  V during a deposition time of 30 s.

A well-defined Hg(II) stripping peak, that increased proportionally with the concentration of the metal ion, arose. The adopted strategy resulted to own a high reproducibility, as the percentage relative standard deviation value on the sensitivity, obtained when performing at least ten calibration curves, was below 9%.

Taking into account the increasing interest in developing a portable device, the applicability of the presented analytical

**TABLE 5** | Interference study of different metal ions on mercury detection (n = 3).

Interferent	Excess	Conventional configuration			Drop configuration		
		$i_{\text{Hg(II)+M(II)}} (\mu\text{A})$	$i_{\text{Hg(II)+M(II)}} / i_{\text{Hg(II)}}$	Signal variation (%)	$i_{\text{Hg(II)+M(II)}} (\mu\text{A})$	$i_{\text{Hg(II)+M(II)}} / i_{\text{Hg(II)}}$	Signal variation (%)
None		0.329 ± 0.021	1.00	-	0.046 ± 0.002	1.00	-
Cd(II)	100	0.424 ± 0.021	1.29	+ 29	0.060 ± 0.003	1.31	+ 31
	500	0.392 ± 0.015	1.19	+ 19	0.064 ± 0.003	1.39	+ 39
Cu(II)	100	0.829 ± 0.016	2.52	+ 152	0.055 ± 0.002	1.19	+ 19
	500	0.816 ± 0.018	2.48	+ 148	0.048 ± 0.001	1.04	+ 4
Pb(II)	100	0.612 ± 0.024	1.86	+ 86	0.080 ± 0.001	1.74	+ 74
	500	0.582 ± 0.022	1.77	+ 77	0.077 ± 0.002	1.67	+ 67
Zn(II)	100	0.355 ± 0.019	1.08	+ 8	0.051 ± 0.002	1.11	+ 11
	500	0.352 ± 0.018	1.07	+ 7	0.044 ± 0.002	0.95	- 5

**TABLE 6** | Figures of merit of mercury calibration curves obtained in complex matrices derived from novel food samples (n = 3).

	Red algae			Brown algae		House cricket flour
	<i>P. dioica</i>	<i>P. yezoensis</i> (Nori)	<i>P. Pal-mata</i>	<i>U. Pinnatifida</i> (Wakame)	<i>A. nodosum</i>	<i>A. domesticus</i>
Sensitivity (mA·L/g)	3.2	2.8	3.0	2.5	2.3	1.5
R <sup>2</sup>	0.9987	0.9985	0.9969	0.9974	0.9956	0.9873
%RSD <sub>max</sub>	15.8	16.5	14.7	18.6	19.2	20.3
Recovery (%)	87–107	76–93	82–100	68–83	63–77	41–50

procedure was proven even in drop configuration for on spot rapid analysis. The decrease in the sensitivity retrieved for mercury determination in these conditions was counterbalanced by an enhancement of the reproducibility and a widening of the linear range: these results were simply retrieved by just increasing the deposition time to 180 s without reaching the saturation of the surface.

Mercury was detected by the presented sensor not only in standard solutions but also in complex matrices as those deriving from novel food samples (e.g., algae and house cricket), in a short analysis time of around 1 min for the conventional and 3.5 mins for drop configuration. As the analyzed algae were obtained from local markets and are thus intended for human consumption, we expected then to find a low amount or even no mercury content; a similar reasoning could be made for house cricket flour, which was not obtained from local markets but derived from animals fed with the

previous kind of algae: therefore, the authors had deemed appropriate to spike these matrices with Hg(II) standard solutions, so that to give a proof of concept of mercury detection in novel foods, which could open the way to further studies to be performed on mercury-contaminated samples.

Therefore, the enhancement of reproducibility and sensitivity given by the developed nanocomposite, together to the native advantages of screen-printed electrodes such as low-cost, disposability, portability, etc., make the modified GSPEs well suited for their future implementation in the determination of the amount of mercury contained in real samples, as the tested novel foods.

#### Author Contributions

**Conceptualization:** Giovanna Marrazza; **Methodology:** Giulia Selvolini; **Formal analysis and investigation:** Sara Failli, Ilaria Antonia

Vitale; **Writing - original draft preparation:** Ilaria Antonia Vitale; **Writing - review and editing:** Giulia Selvolini, Cristina Truzzi, Giovanna Marrazza; **Resources:** Cristina Truzzi, Giovanna Marrazza; **Supervision:** Giovanna Marrazza; **Visualization:** Giulia Selvolini.

### Acknowledgments

The authors did not receive support from any organization for the submitted work. Open access publishing facilitated by Università degli Studi di Firenze, as part of the Wiley - CRUI-CARE agreement. [Correction added on 22 October 2024, after first online publication: Article has been corrected for errors.]

### Conflicts of Interest

The authors declare no conflicts of interest.

### Data Availability Statement

Data sharing is not applicable to this article as no new data were created or analyzed in this study.

### References

1. M. C. Mendes, S. Navalho, A. Ferreira, C. Paulino, D. Figueiredo, D. Silva, et al., *Foods* 11 (2022), DOI: [10.3390/FOODS11131871/S1](https://doi.org/10.3390/FOODS11131871/S1).
2. EFSA (European Food Safety Authority), “Novel food,” can be found under <https://www.efsa.europa.eu/en/topics/topic/novel-food>, 2024.
3. European Parliament, Council of the European Union, *Off. J. Eur. Union* 43 (1997): 1–6.
4. European Parliament, Council of the European Union, *Official Journal of the European Union* 327 (2015): 1–22.
5. R. Roma, G. O. Palmisano and A. De Boni, “Insects as Novel Food: A Consumer Attitude Analysis through the Dominance-Based Rough Set Approach”, *Foods* 9 (2020): 387, <https://doi.org/10.3390/foods9040387>.
6. M. Samarasinghe, K. F. Chai and W. N. Chen, “Forward-looking risk assessment framework for novel foods”, *Food Humanit.* 1 (2023): 500–513, <https://doi.org/10.1016/j.foohum.2023.06.020>.
7. B.-J. Ye, B.-G. Kim, M.-J. Jeon, S.-Y. Kim, H.-C. Kim, T.-W. Jang, H.-J. Chae, W.-J. Choi, M.-N. Ha and Y.-S. Hong, “Evaluation of mercury exposure level, clinical diagnosis and treatment for mercury intoxication”, *Annals of Occupational and Environmental Medicine* 28 (2016): 5, <https://doi.org/10.1186/s40557-015-0086-8>.
8. P. Qu, M. Pang, P. Wang, X. Ma, Z. Zhang, Z. Wang and Y. Gong, “Bioaccumulation of mercury along continuous fauna trophic levels in the Yellow River Estuary and adjacent sea indicated by nitrogen stable isotopes”, *Journal of Hazardous Materials* 432 (2022): 128631, <https://doi.org/10.1016/j.jhazmat.2022.128631>.
9. C. Truzzi, A. Annibaldi, F. Girolametti, L. Giovannini, P. Riolo, S. Ruschioni, I. Olivotto, and S. Illuminati, “A Chemically Safe Way to Produce Insect Biomass for Possible Application in Feed and Food Production”, *International Journal of Environmental Research and Public Health* 17 (2020): 2121, <https://doi.org/10.3390/ijerph17062121>.
10. C. Truzzi, S. Illuminati, F. Girolametti, M. Antonucci, G. Scarponi, S. Ruschioni, P. Riolo and A. Annibaldi, “Influence of Feeding Substrates on the Presence of Toxic Metals (Cd, Pb, Ni, As, Hg) in Larvae of *Tenebrio molitor*: Risk Assessment for Human Consumption”, *International Journal of Environmental Research and Public Health* 16 (2019): 4815, <https://doi.org/10.3390/ijerph16234815>.
11. J. Holmes, P. Pathirathna and P. Hashemi, “Novel frontiers in voltammetric trace metal analysis: Towards real time, on-site, in situ measurements”, *TrAC Trends in Analytical Chemistry* 111 (2019): 206–219, <https://doi.org/10.1016/j.trac.2018.11.003>.
12. R. D. Lama, K. Charlson, A. Anantharam and P. Hashemi, “Ultra-fast Detection and Quantification of Brain Signaling Molecules with

Carbon Fiber Microelectrodes”, *Analytical Chemistry* 84 (2012): 8096–8101, <https://doi.org/10.1021/ac301670h>.

13. M. Li, Y.-T. Li, D.-W. Li and Y.-T. Long, “Recent developments and applications of screen-printed electrodes in environmental assays—A review”, *Analytica Chimica Acta* 734 (2012): 31–44, <https://doi.org/10.1016/j.aca.2012.05.018>.

14. E. Bernalte, C. M. Sánchez and E. P. Gil, “Determination of mercury in ambient water samples by anodic stripping voltammetry on screen-printed gold electrodes”, *Analytica Chimica Acta* 689 (2011): 60–64, <https://doi.org/10.1016/j.aca.2011.01.042>.

15. E. S. Almeida, E. M. Richter and R. A. A. Munoz, “On-site fuel electroanalysis: Determination of lead, copper and mercury in fuel bioethanol by anodic stripping voltammetry using screen-printed gold electrodes”, *Analytica Chimica Acta* 837 (2014): 38–43, <https://doi.org/10.1016/j.aca.2014.05.031>.

16. T. F. Tormin, R. R. Cunha, R. A. B. Da Silva, R. A. A. Munoz and E. M. Richter, “Combination of screen-printed electrodes and batch injection analysis: A simple, robust, high-throughput, and portable electrochemical system”, *Sensors Actuators B Chemical* 202 (2014): 93–98, <https://doi.org/10.1016/j.snb.2014.04.096>.

17. D. Martín-Yerga and A. Costa-García, “Recent advances in the electrochemical detection of mercury”, *Current Opinion in Electrochemistry* 3 (2017): 91–96, <https://doi.org/10.1016/j.coelec.2017.06.012>.

18. W. Liu, Y. Wang, F. Sheng, B. Wan, G. Tang and S. Xu, “A nucleic acid dye-enhanced electrochemical biosensor for the label-free detection of Hg<sup>2+</sup> based on a gold nanoparticle-modified disposable screen-printed electrode”, *Analytical Methods* 14 (2022): 3451–3457, <https://doi.org/10.1039/D2AY00548D>.

19. I. T. Somé, A. K. Sakira, D. Mertens, S. N. Ronkart and J. M. Kauffmann, “Determination of groundwater mercury (II) content using a disposable gold modified screen printed carbon electrode”, *Talanta* 152 (2016): 335–340, <https://doi.org/10.1016/j.talanta.2016.02.033>.

20. A. Karapa, C. Kokkinos, P. R. Fielden, S. J. Baldock, N. J. Goddard and A. Economou, “Gold nanoparticle-modified sustainable plastic sensor chip for voltammetric monitoring of Hg(II)”, *Talanta* 265 (2023): 124850, <https://doi.org/10.1016/j.talanta.2023.124850>.

21. X. Chen, Z. Yi, G. Peng, Z. Yuan, R. Wang and Y. Li, “In-situ deposition of gold nanoparticles on screen-printed carbon electrode for rapid determination of Hg<sup>2+</sup> in water samples”, *International Journal of Electrochemical Science* 19 (2024): 100544, <https://doi.org/10.1016/j.ijoes.2024.100544>.

22. A. L. Suherman, E. E. L. Tanner and R. G. Compton, “Recent developments in inorganic Hg<sup>2+</sup> detection by voltammetry”, *TrAC Trends Analytical Chemistry* 94 (2017): 161–172, <https://doi.org/10.1016/j.trac.2017.07.020>.

23. V. Somerset, E. Iwuoha and L. Hernandez, “Stripping Voltammetric Measurement of Trace Metal Ions at Screen-printed Carbon and Carbon Paste Electrodes”, *Procedia Chemistry* 1 (2009): 1279–1282, <https://doi.org/10.1016/j.proche.2009.07.319>.

24. V. Somerset, J. Leaner, R. Mason, E. Iwuoha and A. Morrin, “Determination of inorganic mercury using a polyaniline and polyaniline-methylene blue coated screen-printed carbon electrode”, *International Journal of Environmental Analytical Chemistry* 90 (2010): 671–685, <https://doi.org/10.1080/03067310902962536>.

25. V. S. Somerset, L. H. Hernandez and E. I. Iwuoha, “Stripping voltammetric measurement of trace metal ions using screen-printed carbon and modified carbon paste electrodes on river water from the Eerste-Kuils River System”, *Journal of Environmental Science and Health Part A* 46 (2011): 17–32, <https://doi.org/10.1080/10934529.2011.526075>.

26. E. C. Okpara, O. E. Fayemi, E. S. M. Sherif, P. S. Ganesh, B. E. K. Swamy and E. E. Ebenso, “Electrochemical evaluation of Cd<sup>2+</sup> and Hg<sup>2+</sup> ions in water using ZnO/Cu<sub>2</sub>ONPs/PANI modified SPCE



- electrode”, *Sensing Bio-Sensing Research* 35 (2022): 100476, <https://doi.org/10.1016/j.sbsr.2022.100476>.
27. R. K. Gupta, R. A. Singh and S. S. Dubey, “Removal of mercury ions from aqueous solutions by composite of polyaniline with polystyrene”, *Separation and Purification Technology* 38 (2004): 225–232, <https://doi.org/10.1016/j.seppur.2003.11.009>.
28. M. V. B. Krishna, D. Karunasagar, S. V. Rao and J. Arunachalam, “Preconcentration and speciation of inorganic and methyl mercury in waters using polyaniline and gold trap-CVAAS”, *Talanta* 68 (2005): 329–335, <https://doi.org/10.1016/j.talanta.2005.08.066>.
29. H. K. Kordasht, M. Hasanzadeh, F. Seidi and P. M. Alizadeh, “Poly (amino acids) towards sensing: Recent progress and challenges”, *TrAC Trends in Analytical Chemistry* 140 (2021): 116279, <https://doi.org/10.1016/j.trac.2021.116279>.
30. T. Kokab, A. Shah, F. J. Iftikhar, J. Nisar, M. S. Akhter and S. B. Khan, “Amino Acid-Fabricated Glassy Carbon Electrode for Efficient Simultaneous Sensing of Zinc(II), Cadmium(II), Copper(II), and Mercury(II) Ions”, *ACS Omega* 4 (2019): 22057–22068, <https://doi.org/10.1021/acsomega.9b03189>.
31. European Parliament, Council of the European Union, *Official Journal of the European Union* 30 (2022): 108–113.
32. N. Elgrishi, K. J. Rountree, B. D. McCarthy, E. S. Rountree, T. T. Eisenhart and J. L. Dempsey, “A Practical Beginner’s Guide to Cyclic Voltammetry”, *Journal of Chemical Education* 95 (2018): 197–206, <https://doi.org/10.1021/acs.jchemed.7b00361>.
33. E. P. Randviir, “A cross examination of electron transfer rate constants for carbon screen-printed electrodes using Electrochemical Impedance Spectroscopy and cyclic voltammetry”, *Electrochimica Acta* 286 (2018): 179–186, <https://doi.org/10.1016/j.electacta.2018.08.021>.
34. B. Ajdini, I. Biancarosa, G. Cardinaletti, S. Illuminati, A. Annibaldi, F. Girolametti, et al., “The use of seaweed as sustainable feed ingredient for the house cricket (*Acheta domestica*): investigating cricket performance and nutritional composition”, *Journal of Insects as Food Feed* (2024): 1–18, <https://doi.org/10.1163/23524588-20230176>.
35. Z. Yu, X. Li, X. Wang, X. Ma, X. Li and K. Cao, “Voltammetric determination of dopamine and norepinephrine on a glassy carbon electrode modified with poly (L-aspartic acid)”, *Journal of Chemical Science* 124 (2012): 537–544, <https://doi.org/10.1007/s12039-011-0179-z>.
36. M. Tudorache and C. Bala, “Biosensors based on screen-printing technology, and their applications in environmental and food analysis”, *Analytical and Bioanalytical Chemistry* 388 (2007): 565–578, <https://doi.org/10.1007/s00216-007-1293-0>.
37. G. Selvolini and G. Marrazza, “On spot detection of nickel and cobalt from exhausted batteries by a smart electrochemical sensor”, *Talanta* 253 (2023): 123918, <https://doi.org/10.1016/j.talanta.2022.123918>.